Japanese Journal of Applied Physics

RAPID COMMUNICATION

Improvement of perovskite solar cell performance by oleylamine treatment of CuSCN hole-transport layer

Japanese Journal of Applied Physics **62**, 050902 (2023) **RAPID COMMUNICATION**
https://doi.org/10.35848/1347-4065/accda6

Improvement of perovskite solar cell performance by oleylamine treatment of CuSCN hole-transport layer

Yuto Komazawa[1], Shiro Uchida[1], Takurou N. Murakami[2], and Atsushi Kogo[2*]

[1]*Chiba Institute of Technology (CIT), 2-17-1 Tsudanuma, Narashino, Chiba 275-0016, Japan*
[2]*National Institute of Advanced Industrial Science and Technology (AIST), 1-1-1 Higashi, Tsukuba, Ibaraki 305-8565, Japan*

[*]E-mail: kogo.atsushi@aist.go.jp

Received February 21, 2023; revised March 23, 2023; accepted April 16, 2023; published online May 2, 2023

Post-treatment of perovskite solar cells with CuSCN hole-transport layers to enhance their photovoltaic performance was investigated. Crystallinity and uniformity of CuSCN layers were improved by recrystallisation caused by oleylamine (OA) treatment. Further, the OA adsorbed on CuSCN tuned the VB edge potential and improved the hole extraction from perovskite materials. Power conversion efficiency of the CuSCN-based perovskite solar cells improved from 8.58% to 11.4%. © 2023 The Japan Society of Applied Physics

Supplementary material for this article is available online

Organometallic halide perovskite materials have attracted enormous attention as light absorbers for solar cells.[1–3] Their strong light absorption in the visible range and long photocarrier diffusion length ($\sim\mu$m)[4] are favourable for obtaining high-performance solar cells. The power conversion efficiency (PCE) of perovskite solar cells (PSCs) reached 25.7%, which is close to that of Si solar cells (26.7%).[5,6] Additionally, low process temperature and solution processability of perovskite materials enable roll-to-roll mass production of solar cells using flexible substrates,[7–11] leading to a significant decrease in fabrication cost. Furthermore, the tuneable band gap energy of perovskites by ion composition[12] makes them applicable to tandem solar cells.[13–15]

However, PSCs face serious challenges in terms of their stability for practical applications. Organic semiconductors, such as 2,2′,7,7′-tetrakis(N,N-di-p-methoxyphenylamino)-9,9′-spirobifluorene (spiro-OMeTAD), are used as hole-transport layers to fabricate PSCs with high PCE by solution processing. However, such organic materials can be easily degraded by light,[16,17] heat,[18–20] and humidity,[18,20,21] resulting in PSCs with low stability.

To address this issue, inorganic and cost-effective CuSCN hole-transport materials (HTMs) have been developed for PSCs.[22–27] The inorganic CuSCN-based PSCs exhibited higher stability than conventional spiro-OMeTAD-based PSCs owing to the robustness of CuSCN.

However, CuSCN-based PSCs have a lower photovoltaic performance (PCE of 15%–20%) than spiro-OMeTAD-based PSCs (>20%). These low performances were due to the poor crystallinity and morphology of CuSCN which had many defects, leading to carrier recombination losses. Currently, to improve the performance of CuSCN-based PSCs, the composition of perovskite[23] and modification of the perovskite-HTM interface[24–26] have been studied to decrease charge-recombination loss. However, controlling the crystallinity and morphology of CuSCN is challenging, and it is essential to obtain a highly crystalline CuSCN layer with high coverage on the perovskite surfaces to avoid shunting to enhance the PSC performance.

Recently, we have found that aging CuSCN at high humidity improved crystallinity and photovoltaic performance of PSCs.[27] In this study, we focused on controlling the crystallinity and electrical properties of CuSCN by post-treatment, which is easier than controlling humidity, to further improve CuSCN crystallinity and enhance the photovoltaic performance of CuSCN-based PSCs. We employed oleylamine (OA), which is an amphiphilic material that is usually used as a surfactant to dissolve inorganic semiconductor nanoparticles in organic solvents,[28] to induce recrystallisation of CuSCN crystals.

The surface of the CuSCN layers was dissolved and recrystallised using 2-propanol containing OA, and the crystallinity and uniformity of the layer was improved. Moreover, the electron band shift of CuSCN caused by electron donation from adsorbed OA improved the hole extraction from perovskite materials. The dark current density was suppressed by an order of magnitude to improve the open-circuit voltage (V_{OC}) by 13%. Consequently, the PCE of the CuSCN-based PSCs improved from 8.58% to 11.4%.

The CuSCN-based PSCs were fabricated as follows. Indium tin oxide (ITO)-coated glass substrates were treated with UV ozone. A SnO_2 colloidal solution (44592, Alfa Aesar) was spin-coated on the substrates at 2000 rpm for 30 s and dried at 150 °C for 1 h to form SnO_2 electron collector. The ITO/SnO_2 substrates were cleaned again by UV ozone treatment (20 min), and $Cs_{0.05}(FA_{0.83}MA_{0.17})_{0.95}Pb(I_{0.83}Br_{0.17})_3$ (FA = $CH(NH_2)_2$, MA = CH_3NH_3) perovskite[29] was deposited in dry air (dew point −30 °C). FAI (1 M), MABr (0.2 M), PbI_2 (1.1 M), and $PbBr_2$ (0.2 M) were dissolved in a mixed solvent of anhydrous N,N-dimethylformamide, and dimethyl sulfoxide (DMSO) (volume ratio of 4:1) with a 4 vol% additive of CsI (1.5 M) in DMSO. The solution was spin-coated on the substrates through a two-step programme of 1000 rpm for 10 s and 4000 rpm for 30 s. To induce perovskite crystallisation, chlorobenzene was poured on the substrate 20 s before the end of the spin-coating, and the substrates were annealed at 105 °C for 1 h. A diethyl sulfide solution containing 80 mg ml^{-1} CuSCN was spin-coated at 6000 rpm for 30 s in ambient atmosphere. OA dissolved in 2-propanol (25 mM) was spin-coated on the substrates at 6000 rpm for 30 s and dried at 80 °C for 5 min in ambient air. The substrates were aged overnight in dry air. Au electrodes were then formed by vacuum deposition on substrates (3 × 3 mm). The photoelectric conversion characteristics of the PSCs were evaluated under 1-sun illumination using a solar simulator (WXS-80C-3, WACOM) through a black mask (aperture size = 3 × 3 mm) with a source meter (R6243, ADVANTEST) in ambient air at RT (scan speed =

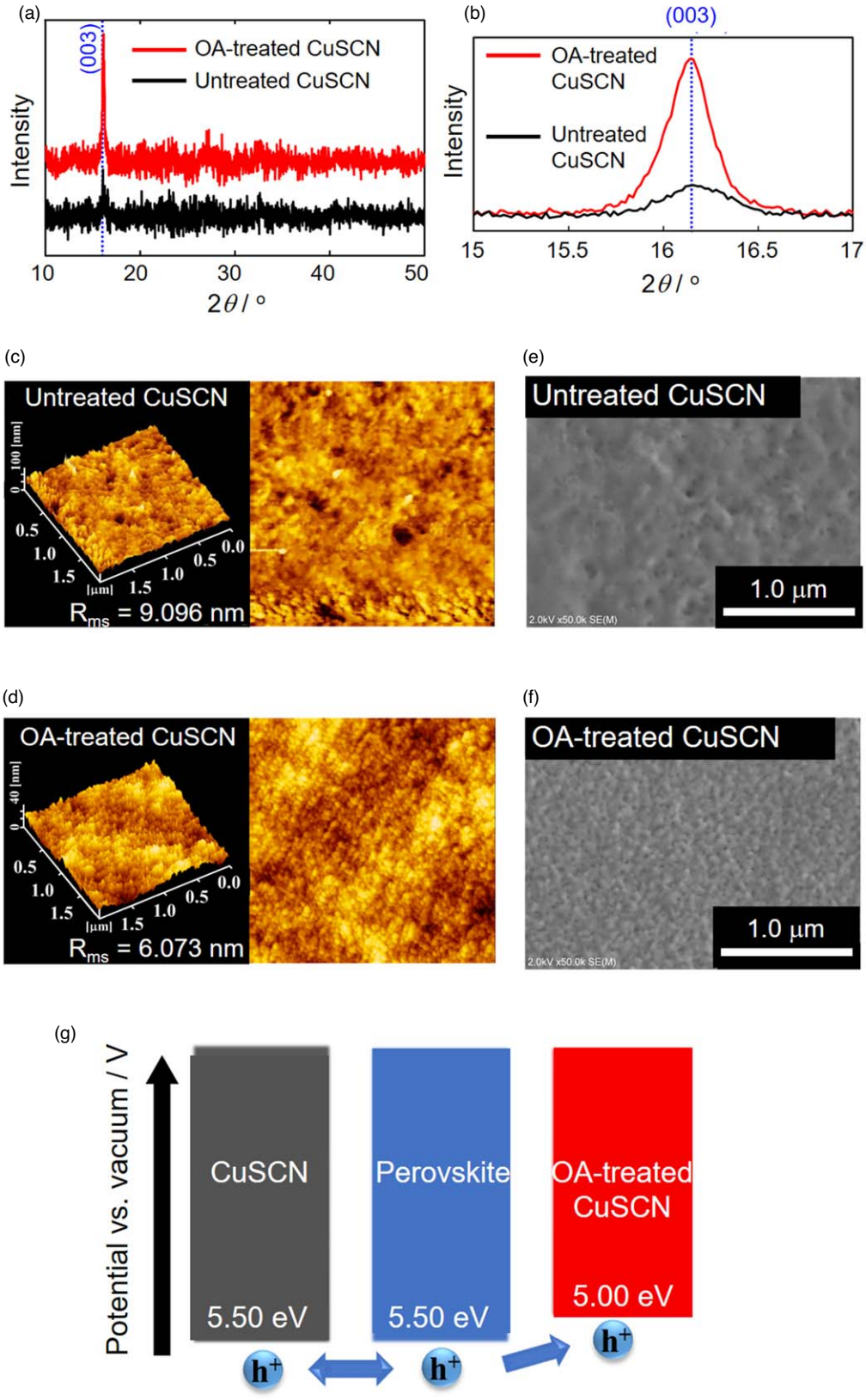

Fig. 1. X-ray diffractometer pattern of the CuSCN film in the range of (a) $2\theta = 10°$–$50°$ and (b) $2\theta = 15.5°$–$17.0°$. (c), (d) AFM images and (e), (f) SEM images of the CuSCN film. (g) VB edge potential of perovskite and CuSCN.

0.1 V s^{-1}, dwell time = 0.05 s). To adjust the incident intensity, a reference crystal Si cell (J-NIMC01, calibrated and certificated by Japan Quality Assurance Organization) was used.

An X-ray diffractometer (SmartLab, Rigaku) with a CuKα source, scanning electron microscope (SEM) (S4800, HITATHI), atomic force microscope (NanoNavi, HITACHI), photoelectron-yield spectroscopy system (PYS; BIP-KV200, Bunko Keiki), and photoluminescence (PL) spectrometer (C12132, Hamamatsu Photonics) were used for characterisation.

The results of the X-ray crystallographic analysis of the CuSCN films formed on glass substrates are shown in

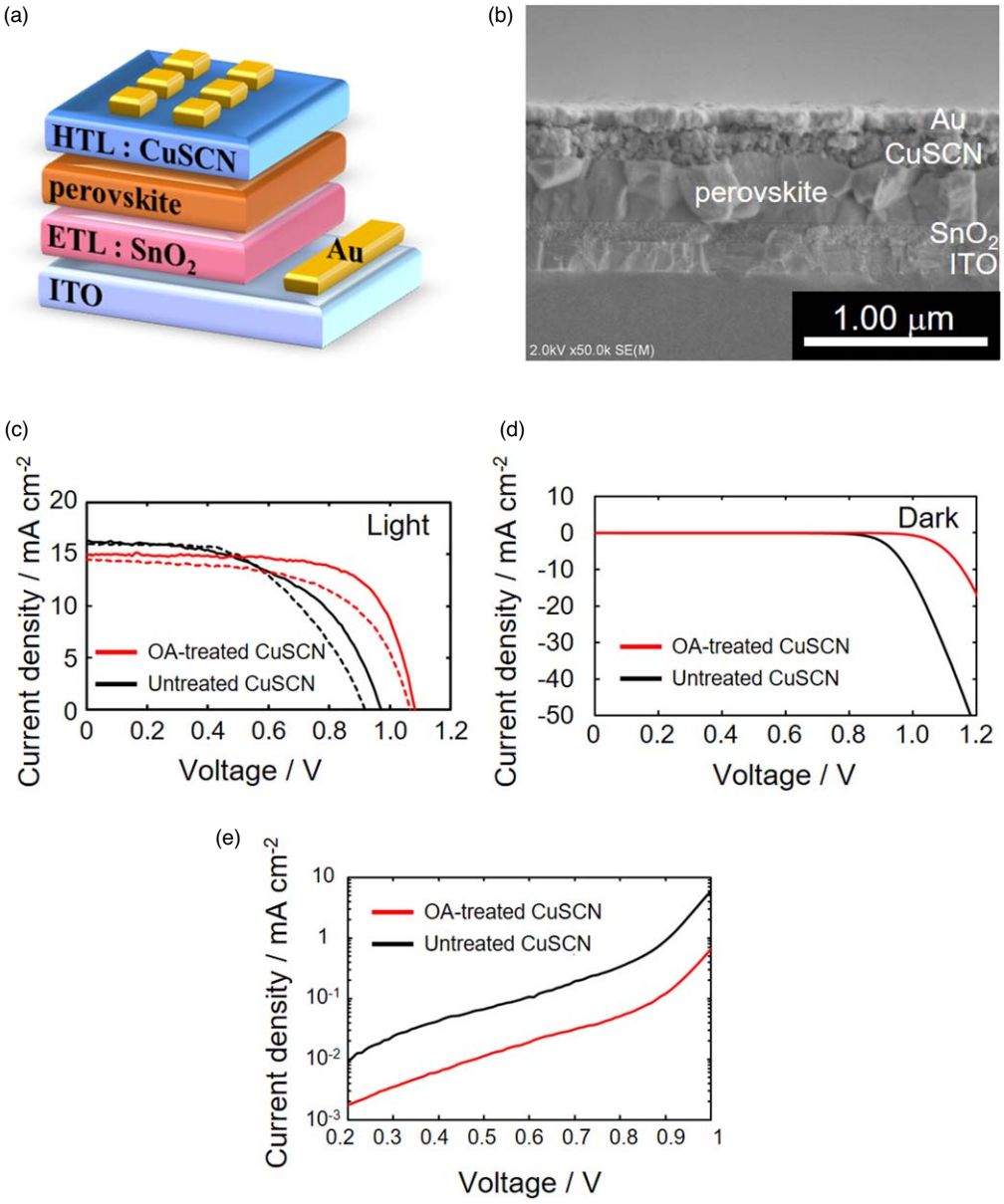

Fig. 2. (a) Schematic and (b) cross-sectional SEM image of solar cells used for *J*–*V* analysis, *J*–*V* curves of the CuSCN-based PSCs measured under 1-Sun illumination (c) and in dark (d), (e). Forward (−0.2 V → 1.3 V) and backward (1.3 V → −0.2 V) voltage scans are indicated with solid and dashed line, respectively.

Table I. Solar cell parameters of CuSCN-based PSCs (scan direction −0.2 V → 1.3 V). Data were collected for no less than 9 cells.

HTL	J_{sc}/mA cm^{-2}	V_{oc}/V	FF	PCE/%
Untreated CuSCN	16.34 ± 0.93	0.96 ± 0.03	0.549 ± 0.032	8.58 ± 0.23
OA-treated CuSCN	14.94 ± 0.34	1.08 ± 0.04	0.704 ± 0.020	11.4 ± 0.62

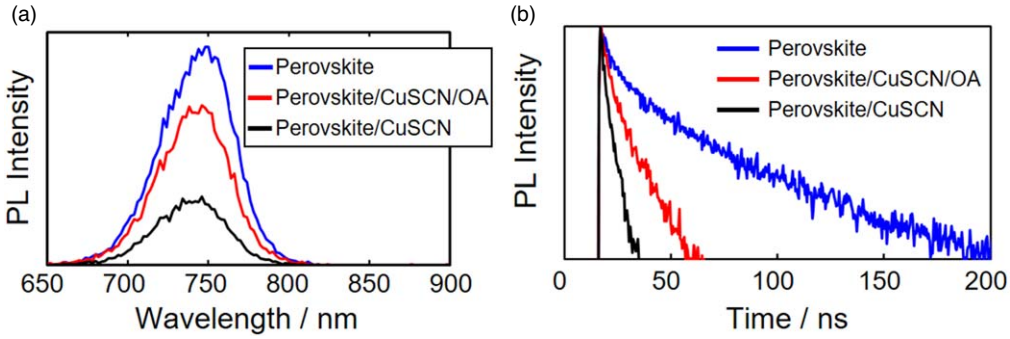

Fig. 3. (a) PL spectrum and (b) PL intensity decay (wavelength; 750 nm) of glass/perovskite/CuSCN substrates (incident wavelength 532 nm, 0.51 mW).

Figs. 1(a), 1(b). Diffraction peaks at 16.1°, which correspond to diffraction at the (003) plane of CuSCN[30] were observed. The peak intensity was significantly increased by OA treatment, suggesting improved crystallinity of the CuSCN. The CuSCN crystal size was estimated from width of the peak using the Scherrer equation. The crystal size of CuSCN treated with OA was 37.1 nm and that without OA treatment was 21.4 nm. This indicates that OA dissolved amorphous surface of CuSCN and induced the recrystallisation. The rms roughness (R_{ms}) values of the OA-treated CuSCN surface estimated by atomic force microscope (AFM) [Fig. 1(d)] was 6.1 nm, which is smaller than that of untreated CuSCN [Fig. 1(c), R_{ms} = 9.1 nm]. This suggests that the OA treatment dissolved and recrystallised the CuSCN surface. SEM observations [Figs. 1(e), 1(f)] indicate that recrystallisation by OA treatment reduced the size and number of pinholes and defects.

PYS measurements were performed on CuSCN and perovskite formed on ITO substrates to determine the VB edge potentials [Fig. 1(g)]. The VB edge potentials of the CuSCN and perovskite films were similar at 5.50 eV. The potential of the OA-treated CuSCN film was 5.00 eV, indicating that the electron-donating ability of OA adsorbed on CuSCN shifted the VB edge.

The structure and cross-sectional SEM images of the CuSCN-based PSCs are shown in Figs. 2(a), 2(b). The thicknesses of the SnO_2, perovskite, and CuSCN layers were 100, 400, and 250 nm, respectively. We estimated solar cell parameters (Table I and Table SI for −0.2 V → 1.3 V and 1.3 V → −0.2 V voltage scan) from *J*–*V* curves measured under 1-Sun illumination [Fig. 2(c)]. The PSCs with OA treatment exhibited a higher PCE of 11.4% than those without treatment (8.6%) owing to the improvement in V_{OC} and fill factor (FF).

The onset voltage of the dark *J*–*V* curve was larger for OA-treated PSCs than for untreated PSCs, indicating that the electron rectification was improved by the decreased pinholes and defects on CuSCN [Fig. 2(d)]. Furthermore, the OA-treated PSCs exhibited a smaller current density in the low-voltage range (<0.8 V) owing to the low trap density [Fig. 2(e)]. CuSCN recrystallisation caused by OA treatment decreased the trap density, improved carrier rectification, and enhanced V_{OC} and FF. Moreover, the improved crystallinity of the CuSCN film and the electron band shift caused by the OA treatment are considered to have reduced the resistance through the CuSCN film and the CuSCN/perovskite interface for hole extraction.

To investigate the carrier dynamics of the perovskite/CuSCN interface, we performed PL analysis on the glass/perovskite/CuSCN substrates. Fig. 3(a) shows the PL emission spectra, and Fig. 3(b) shows the PL intensity decay (wavelength: 750 nm). Peaks at ∼750 nm were observed for all substrates. This wavelength corresponds to the band gap wavelength of perovskite, suggesting that the PL was due to radiative recombination in the perovskite layers. We compared the PL intensity decay of perovskites with that of glass/perovskite and glass/perovskite/CuSCN substrates [Fig. 3(b)]. The PL intensity decay of the glass/perovskite/CuSCN substrates was faster than that of the glass/perovskite substrate, owing to the hole extraction of CuSCN. Compared to the untreated CuSCN substrate, the OA-treated glass/perovskite/CuSCN substrates exhibited a stronger PL intensity [Fig. 3(a)] and longer PL lifetime [Fig. 3(b)]. The PL intensity and lifetime of perovskite are reduced not only by hole extraction to CuSCN but also by non-radiative recombination in the perovskite and at the interface. Therefore, the large PL intensity and longer PL lifetime of the OA-treated glass/perovskite/CuSCN can be ascribed to the reduction in traps at the perovskite/CuSCN interface, which suppressed non-radiative recombination.

In conclusion, we treated a CuSCN hole-transport layer with an OA solution to improve the photovoltaic performance of PSCs. OA treatment of CuSCN improved the crystallinity and yielded uniform CuSCN layers. Furthermore, the electron-donating nature of OA shifts the VB edge of CuSCN to improve hole extraction from the perovskite. PSCs with OA-treated CuSCN exhibited a larger PCE than those without OA treatment, improving V_{OC} and FF.

Acknowledgments This research was financially supported by a Grant-in-Aid for Early-Career Scientists (21K14733) from the Japan Society for the Promotion of Science (JSPS) and the New Energy and Industrial Technology Development Organization (NEDO).

ORCID iDs Takurou N. Murakami https://orcid.org/0000-0002-2066-3982 Atsushi Kogo https://orcid.org/0000-0002-9837-5585

1) A. Kojima, K. Teshima, Y. Shirai, and T. Miyasaka, J. Am. Chem. Soc. **131**, 6050 (2009).
2) M. M. Lee, J. Teuscher, T. Miyasaka, T. N. Murakami, and H. J. Snaith, Science **338**, 643 (2012).
3) H.-S. Kim et al., Sci. Rep. **2**, 591 (2012).
4) Q. Dong, Y. Fang, Y. Shao, P. Mulligan, J. Qiu, L. Cao, and J. Huang, Science **347**, 967 (2015).
5) Efficiency chart of NREL, (https://www.nrel.gov/pv/assets/pdfs/best-research-cell-efficiencies.pdf) (4/5/2023).
6) M. A. Green, E. D. Dunlop, G. Siefer, M. Yoshita, N. Kopidakis, K. Bothe, and X. Hao, Prog. Photovolt. **31**, 3 (2023).
7) B. J. Kim et al., Energy Environ. Sci. **8**, 916 (2015).
8) D. Yang, R. Yang, S. Priya, and S. Liu, Angew. Chem. Int. Ed. **58**, 4466 (2019).
9) A. Kogo, M. Ikegami, and T. Miyasaka, Chem. Commun. **52**, 8119 (2016).
10) A. Kogo, S. Iwasaki, M. Ikegami, and T. Miyasaka, Chem. Lett. **46**, 530 (2017).
11) J. F. Benitez-Rodriguez, D. Chen, M. Gao, and R. A. Caruso, Sol. RRL **5**, 2100341 (2021).
12) S. Tao, I. Schmidt, G. Brocks, J. Jiang, I. Tranca, K. Meerholz, and S. Olthof, Nat. Commun. **10**, 2560 (2019).
13) C. McDonald, H. Sai, V. Svrcek, A. Kogo, T. Miyadera, T. N. Murakami, M. Chikamatsu, Y. Yoshida, and T. Matsui, ACS Appl. Mater. Interfaces **14**, 33505 (2022).
14) R. Lin et al., Nature **603**, 73 (2022).
15) J. Liu et al., Science **377**, 302 (2022).
16) A. L. Palma, L. Ciná, S. Pescetelli, A. Agresti, M. Raggio, R. Paolesse, F. Bonaccorso, and A. D. Carlo, Nano Energy **22**, 349 (2016).
17) R. S. Sanchez and E. Mas-Marza, Sol. Energy Mater. Sol. Cells **158**, 189 (2016).
18) S. N. Habisreutinger, T. Leijtens, G. E. Eperon, S. D. Stranks, R. J. Nicholas, and H. J. Snaith, Nano Lett. **14**, 5561 (2014).
19) T. Malinauskas, D. Tomkute-Luksiene, R. Sens, M. Daskeviciene, R. Send, H. Wonneberger, V. Jankauskas, I. Bruder, and V. Getautis, ACS Appl. Mater. Interfaces **7**, 11107 (2015).
20) G. Ren, W. Han, Y. Deng, W. Wu, Z. Li, J. Guo, H. Bao, C. Liu, and W. Guo, J. Mater. Chem. A **9**, 4589 (2021).
21) G. Niu, X. Guo, and L. Wang, J. Mater. Chem. A **3**, 8970 (2015).
22) N. Arora, M. I. Dar, A. Hinderhofer, N. Pellet, F. Schreiber, S. M. Zakeeruddin, and M. Grätzel, Science **358**, 768 (2017).
23) G. Kim et al., ACS Appl. Mater. Interfaces **14**, 5203 (2022).
24) J. Kim, Y. Lee, A. J. Yun, B. Gil, and B. Park, ACS Appl. Mater. Interfaces **11**, 46818 (2019).
25) V. E. Madhavan, I. Zimmermann, A. A. B. Baloch, A. Manekkathodi, A. Belaidi, N. Tabet, and M. K. Nazeeruddin, Energy Mater. **3**, 114 (2020).
26) M. Lyu, J. Chen, and N.-G. Park, J. Solid State Chem. **269**, 367 (2019).

27) A. Kogo and T. N. Murakami, ChemPhysChem **24**, e202200832 (2023).
28) S. Mourdikoudis and L. M. Liz-Marzán, Chem. Mater. **25**, 1465 (2013).
29) M. Saliba et al., Energy Environ. Sci. **9**, 1989 (2016).
30) Y. Tsuda, K. Uda, M. Chiba, H. Sun, L. Sun, M. S. White, A. Masuhara, and T. Yoshida, Microsyst. Technol. **24**, 715 (2018).